Ab initio insight into the physical properties of new ferroelectric perovskite oxide materials $XGeO_3$ (X= Sr, Ca)

A. Waqdim[1], M. Agouri[1], M. Ouali[1], A. Abbassi[1,*] S. Taj[1], B. Manaut[1,*], and M. El Idrissi[1,2]

[a]*Laboratory of Research in Physics and Engineering Sciences,*
Sultan Moulay Slimane University, Polydisciplinary Faculty, Beni Mellal, 23000, Morocco.
*e-mail: *abbassi.abder@gmail.com; *b.manaut@usms.ma*
[b]*Sultan Moulay Slimane University, Polydisciplinary Faculty of Khouribga.*

Received 23 January 2024; accepted 23 April 2024

The investigation of structural stability, electronic, mechanical, spontanous polarization, and thermodynamic properties of simple cubic perovskite oxides $XGeO_3$ (X =Sr, Ca) has been performed through density functional theory as introduced in Wien2K code. The tolerence factor, Born criteria, and phonon dispersion confirm the stability and the formation of both materials in the ideal cubic structure. Additionally, the application of nmBJ approach in electronic properties shows an exceptional semiconducting aspect. The strain effect on spontaneous polarization of $XGeO_3$ (X =Sr, Ca) perovskites presents an excellent ferroelectric behavior. The thermodynamic parameters such as volume, bulk modulus, thermal expansion coefficient, Debye temperature, Gibbs free energy, enthalpy, heat capacities, and Grüneisen, have been calculated and discussed with a wide range of pressures ($0-20$ GPa) and temperatures ($0-1000$ K). Based on the exceptional semiconducting nature and significant spontaneous polarization, the studied materials can be considered as ferroelectric materials, which make them as a suitable candidates in ferroelctric devices.

Keywords: DFT; perovskite oxides; Wien2K; ferroelectric; nmBJ.

DOI: https://doi.org/10.31349/RevMexFis.70.051603

1. Introduction

The simple perovskite oxides family encompasses a diverse range of materials, ranging from insulator to superconductor aspect. It is characterized by the general chemical formula ABO_3, and the variety of A and B cations can exhibit different properties, based on the valence electrons of each atom [1, 2]. Additionally, these materials hold significant interest in material science owing to their involving material characteristics and adjustable physical properties [3–5]. The simple perovskite oxides are considered as multifunctional, and present different characteristics such as ferroelectricity, high thermoelectric efficiency, and spin polarization [6, 7]. All these rich characteristics are behind a number of applications, including solar cells, spintronic, ferroelectric memories, and optoelectronic applications [8, 9]. Among the perovskites, ferroelectric perovskite oxides are of great interest in photovoltaic applications owing to their significant band gap energy and also their important spontaneous polarization values [10]. Several simple perovskite oxide materials $BaTiO_3$, $PbTiO_3$, $BiZn_{1/2}Ti_{1/2}O_3$, $BiFeO_3$, $PbZrO_3$, $LiNbO_3$, $BaZrO_3$, $CaTiO_3$, $BiXO_3$ (X=Co, Mn, Fe, V, Zn), and $BaHfO_3$ are reported to show a semiconductor behavior and have ferroelectric aspects [11–20]. For example, the $BaTiO_3$ perovskite is considered a ferroelectric material, which is polarized spontaneously. Indeed, the negative and positive charge centers within the crystal do not coincide each other, which is the cause of its electric dipole moment.

Ge-based simple perovskites have been studied for their interesting characteristics. They are also investigated as an alternative material in renewable energy and ferroelectric devices [21]. In addition, many theoretical and experimental studies have been widely carried out on these type of materials. They have several industrial applications in the manufacture of electronic, optoelectronic, thermoelectric, and ferroelectric devices [22, 23]. Simple perovskite oxide $PbGeO_3$ has been experimentally and theoretically reported, that it is crystallized in the ideal cubic structure and also emerged an exceptional semiconducting characteristics [24, 25]. Additionally, N. A. Noor and co-workers [26] theoretically investigated the pressure effect on electronic, optical and thermoelectric properties of cubic perovskite oxide $BaGeO_3$. An indirect to direct band gap transition with a p-type aspect is demonstrated.

Simple perovskite oxides $XGeO_3$ (X=Sr, Ca) are widely studied which can be applied in various devices. Some experimental works lately published affirm that these materials are crystallized in the ideal cubic structure through the high-resolution X-ray diffraction (HR-XRD) [27, 28]. The atomic positions in the elementary cell are X: 1a(0, 0, 0); Ge: 1b(1/2, 1/2, 1/2) and O: 3d(1/2, 1/2, 0). At low temperature, Y. Wang, *et al*. [29] reported that the $SrGeO_3$ has a good conductivity and excellent stability. Additionally, its optoelectronic properties show applicability in the field of photovoltaic and photocatalysis [30]. Furthermore, based on X-ray diffraction study, A. Nakatsuka, *et al*. reported experimentally the excellent stability of the $SrGeO_3$ perovskite phase under high pressure at various temperatures ranging from 100 to 323 K [31]. $CaGeO_3$ has been theoretically investigated through DFT calculation, where the authors have reported that it has a semi-

conductor nature and high thermoelectric performance [32].

All exceptional characteristics observed in Ge-based perovskite oxides can be proposed to goal their application for photovoltaic and ferroelectric devices. For this reason, we investigate the structural, dynamic, and mechanic stabilities, in addition to, electronic, spontaneous polarization, and thermodynamic properties of the proposed cubic perovskite oxides $XGeO_3$ (X=Sr, Ca) by using the Full-Potential Linearized Augmented Plane Wave (FP-LAPW) method implemented in the Wien2k code.

2. Computational details

Studies on the structural stability, mechanical, electronic, spontaneous polarization, and thermodynamic properties of simple perovskite oxides $XGeO_3$ (X= Sr, Ca) have been performed by using the density functional theory (DFT) based on full-potential linearized augmented plane wave (FP-LAPW) implemented in WIEN2K [33–35]. Perdew-Burke-Ernzehof functional for solids within the generalized gradient approximation (GGA-PBEsol) is used for the structural properties [36], while the electronic properties were determined by applying the new modified Becke-Johnson approximation (nmBJ), which is given by [37, 38]:

$$\vartheta_x^{nmBJ}(r) = c\vartheta_x^{BR}(r) + (3c-2)\frac{1}{\pi}\sqrt{\frac{5}{12}}\sqrt{\frac{2E(r)}{\rho(r)}}, \quad (1)$$

where $E(r)$ is the Kohn-Sham kinetic energy density, and $\rho(r)$ is the electron density. The parameter $\vartheta_x^{BR}(r)$ represents the Becke-Roussel (BR) exchange potential. The new parameterization of c is suggested from the density, and it reads:

$$c = \mu + \nu\sqrt{\frac{1}{V_{cell}}\int_{cell}\frac{1}{2}\left(\frac{|\nabla\rho^{\uparrow}(r')|}{\rho_{\uparrow}}+\frac{|\nabla\rho^{\downarrow}(r')|}{\rho_{\downarrow}}\right)dr'^3}, \quad (2)$$

where μ and ν have been chosen according to the experimental band gap fits. Moreover, $R_{MT} * K_{\max} = 7$ is chosen as the number of plane waves in the interstitial region such that R_{MT} is the smallest Muffin-tin radius in the unit cell, and $K_{\max}$ is the maximum of the reciprocal lattice vector. The $(10\times10\times10)$ $k-$points and the tetrahedral method [39] have been used for the Brillouin Zone integration, and the total energies converged below 10^{-5} Ry. The total energies are computed as a function of volume and fitted to the Birch-Murnagan equation of state [40] to get the ground state properties like zero-pressure equilibrium volume. The dynamic stability of the studied materials is checked by calculating the phonon dispersion curve using the Phonopy package [41], embedded in the Wien2k code. The mechanical properties are predicted by investigating their elestic constants, which are calculated throuth ElaStic-1.1 package [42]. Moreover, we focus also on the study of strain effect on spontaneous polarization, based on the Berry phase approach using the BerryPI package [43] which is introduced in the Wien2k code. Based on the results fitted from the BM equation of state, the thermodynamic parameters have been determined using quasi-harmonic Debye model [44, 45], as introduced in the Gibbs2 package [46].

3. Results and discussions

3.1. Structural stability

In this paper, simple perovskite oxides $XGeO_3$ (X= Sr, Ca) have been studied in the cubic model ($Pm\bar{3}m$) as shown in Fig. 1.

The optimization of structural parameters through the unit cell volume is made to obtain the lattice constants, pressure derivative and bulk modulus. The extracted volume depending on the calculated energies is presented by exploitation of Birch-Murnaghan's equation as follows [48]:

$$E(V) = E_0 + \frac{9V_0B}{16}\left(\left[\left(\frac{V_0}{V}\right)^{2/3}-1\right]^2B' + \left[\left(\frac{V_0}{V}\right)^{2/3}-1\right]^2\left[6-4\left(\frac{V_0}{V}\right)^{2/3}\right]\right), \quad (3)$$

where V_0 denotes the volume of the unit cell. E_0 is taken as the minimum energy which is the ground state energy corresponding to the equilibrium volume. B and B' are successively the bulk modulus and its pressure derivative, and they

TABLE I. Computed lattice constant a, volume V_0, Bulk modulus B, its primitive B' and the total ground state energy E_0 of cubic perovskite oxides $XGeO_3$ (X= Sr, Ca), comparing with other works.

Materials	Methods	a(Å)	V_0(Å^3)	$B(GPa)$	$B'(GPa)$	$E_0(Ry)$
$SrGeO_3$	GGA	3.8082	55.2279	186.44	4.6567	-11001.50
[49]	Exp	3.7980	54.785	–	–	–
[50]	Exp	3.7968	54.733	194	–	–
$CaGeO_3$	GGA	3.7934	54.5865	233.0158	5	-6010.86
[51]	GGA	3.807	55.175	180.31	.	-11001.44

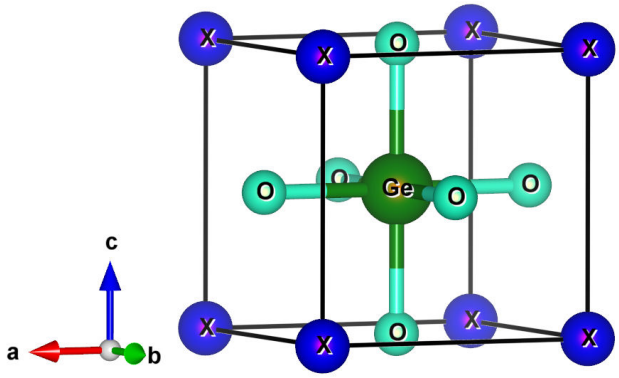

FIGURE 1. Cubic structure of perovskite oxide $XGeO_3$ $(X = Sr,\ Ca)$ [47].

are related to the equilibrium volume of the unit cell. Table I summarizes the obtained structural parameters of $XGeO_3$ (X= Sr, Ca) materials, and also lists some other theoretical and experimental studies, comparing with our results.

To manufacture these materials, it is necessary to validate their formation and their stability. Generally, the stability and formation of perovskite oxides family are widely checked from a theoretical parameter called tolerance factor (T), which is determined by the standard formula [52]:

$$T = \frac{R_X + R_O}{\sqrt{2}(R_{\text{Ge}} + R_O)}, \tag{4}$$

where $R_{(i=X,\ \text{Ge},\ \text{O})}$ presents the ionic radii of each ion. The calculated tolerence factor of $SrGeO_3$ and $CaGeO_3$ materials is equal to 1.04 and 0.911, respectively. Therefore, the obtained tolerance factor values are in the range of 0.9 to 1.1, which fulfil the formation and stability of all proposed materials in the ideal cubic structure [53]. To verify the dynamic stability of our materials, we have computed the phonon dispersions of $XGeO_3$ (X = Sr, Ca) compounds using the finite displacement method implemented in the phonopy package [41]. Figure 2 presents the phonon dispersion curves of both materials. From this figure, we observe that there are no imaginary frequencies in the phonon spectra, confirming the dynamical stability of our materials in a cubic phase. Furthermore, our findings align with those of other studies [54, 55].

In terms of theoretical stability, which encompasses Goldsmith's tolerance factor and phonon dispersion, simple perovskite oxide materials $XGeO_3$ (X = Sr, Ca) demonstrate notable stability in their ideal cubic phase. A study conducted by A. Nakatsuka *et al*. utilized X-ray diffraction to experimentally confirm the structural stability of these materials across temperatures ranging from 100 to 323 K. Additionally, they observed excellent crystal stability, with the materials maintaining high cubic symmetry even at low temperatures. These theoretical insights, corroborated by experimental findings, indicate that perovskites $XGeO_3$ (X = Sr, Ca) hold promise for maintaining stability in their ideal cubic structure [31, 56].

3.2. Elastic and mechanical properties

To understand the mechanical behavior of a material, we should calculate its elastic properties. They are important features that play a key role in material sciences and novel technology. Moreover, these elastic properties enable us to know the capability of a material to be distorted during the strain effects (stress, force...), and they also help in the estimation of the stability of a material. To explore these materials stability, such as strength, hardness or softness, etc, we have calculated the elastic constants of $XGeO_3$ (X= Sr, Ca) materials using the ElaStic1.1 package performed in the WIEN2k code. These elastic constants have been described by three independent elastic parameters which are denoted by C_{11}, C_{12}, and C_{44}. The mechanical stability is checked by using Born criteria that are given by [57, 58]:

$$\begin{aligned} &C_{11} + 2C_{12} > 0\ ,\ \ C_{11} - C_{12} > 0\ \ , \\ &C_{44} > 0,\ \ \text{and}\ \ C_{12} < B < C_{11}. \end{aligned} \tag{5}$$

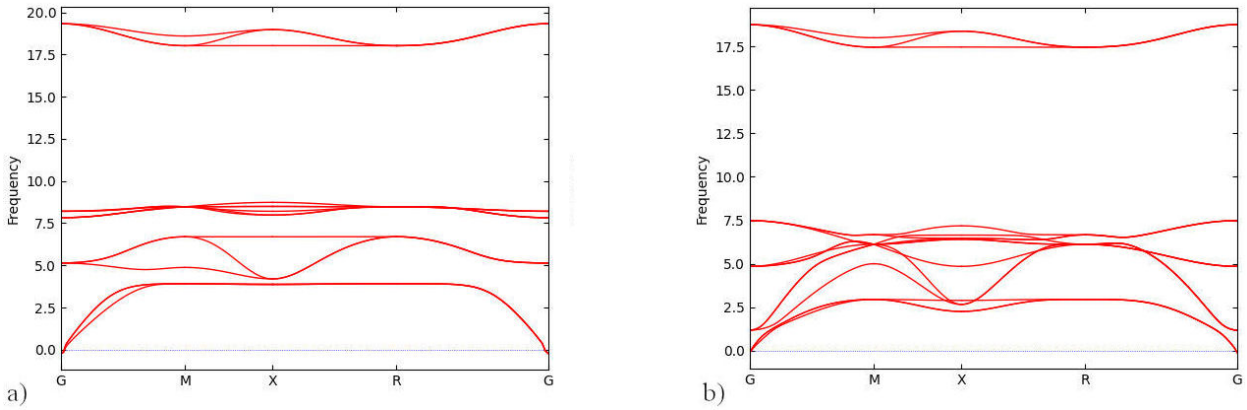

FIGURE 2. Phonon dispersions of cubic perovskite oxides $SrGeO_3$ a) and $CaGeO_3$ b) compounds.

TABLE II. The calculated elastic constants of cubic $XGeO_3$ (X=Sr, Ca) perovskite oxides, comparing with other perovskite elements.

Parameters	$SrGeO_3$	$CaGeO_3$	[49]	[51]
C_{11}(GPa)	328.5	291.3	305.39	243.39
C_{12}(GPa)	121.1	114.6	114.68	112.78
C_{44}(GPa)	156.5	128.0	145.99	130.12

From these constants, we can derive the mechanical parameters such as bulks modulus (B), Young's modulus (Y), anisotropic factor (A), Poisson's ratio (ν) and Hill's shear modulus (G), which is an arithmetic average of the (G_R) Reuss and (G_V) Voigt approximation, by using the equations [59–61]:

$$B = \frac{C_{11} + 2C_{12}}{3}, \tag{6}$$

$$Y = \frac{9GB}{G + 3B}, \tag{7}$$

$$G = \frac{G_V + G_R}{2}, \tag{8}$$

$$G_V = \frac{C_{11} - C_{12} + 3C_{44}}{5}, \tag{9}$$

$$G_R = \frac{5C_{44}(C_{11} - C_{12})}{4C_{44} + 3(C_{11} + C_{12})}, \tag{10}$$

$$\nu = \frac{3B - 2G}{2(3B + G)}, \tag{11}$$

$$A = \frac{2C_{44}}{C_{11} - C_{12}}, \tag{12}$$

where G_V and G_R are the shear modulus of the Voight and Reuss approaches, respectively.

The elastic constants of cubic $XGeO_3$ (X= Sr, Ca) materials are presented in Table II. According to this table, the calculated elastic constants of $XGeO_3$ (X= Sr, Ca) respect the Born's criteria, and this result proves that our materials are mechanically stable in the cubic structure. In addition, it is shown that the computed value of C_{11} is higher than C_{12}, indicating the incompressibility along the crystallographic a-axis is larger than that along the b-axis.

Table III presentes the calculated values of bulk modulus B, shear modulus G, Pugh's ratio B/G, Young's modulus Y, Cauchy pressure C'', Poisson's ratio ν and elastic anisotropic factor A of the cubic $XGeO_3$ (X=Sr, Ca) perovskite oxides. The obtained results show that the bulk modulus of $XGeO_3$ (X=Sr, Ca) materials are large which signifies that the materials withstand the changes in volume from all sides whenever they are compressed. In addition, the bulk modulus values of $CaGeO_3$ and $SrGeO_3$ indicate the low compressibility of our materials. The mechanical parameters like Young's modulus (Y) are associated with the physical hardness or stillness behavior of any material. From the Table III, we can observe a high Young's modulus value of $SrGeO_3$ and $CaGeO_3$ equal to 322.98 GPa and 273.13 GPa, respectively. This result proves the rigidity of our materials. The examination of ductility and brittleness of $XGeO_3$ (X=Sr, Ca) materials have been made by evaluating Pugh's ratio (B/G), Poisson's ratio (ν), and Cauchy pressure (C''). The critical value of the B/G ratio which distinguishes between ductility and brittleness is 1.75. Any value of B/G lower than 1.75 is associated with a brittleness aspect, while a higher one is related to the ductility nature [62]. The computed value of B/G is found to be 1.43 for $SrGeO_3$ and 1.57 for $CaGeO_3$ material, which means that our compounds have a brittle nature. This has further been examined also by Cauchy's pressure $(C_{12} - C_{44})$ value, which classifies the material with a ductile or brittle aspect if it is positive or negative, respectively. The computed values of Cauchy pressure are negative for $SrGeO_3$ (-35 GPa) and for $CaGeO_3$ (-13.4 GPa), hence verifying the brittle nature of both materials as shown previously by the B/G ratio. The Poisson's ratio (ν) is also another interesting parameter that can help to confirm the ductile and brittle behavior of a material. In line with the Frantsevich rule, a material will possess brittle nature if the value of ν is lower than 0.26, and ductile nature if the value of ν is larger than 0.26 [63]. According to Table III, the computed values of ν in our case are equal to 0.22 for $SrGeO_3$ and equal to 0.24 for $CaGeO_3$ material, which is inferior to 0.26. This result ensures again that the $XGeO_3$ (X=Sr, Ca) materials have brittle characteristics. As a consequence, all the computed parameters, which are Pugh ratio B/G, Cauchy pressure C'', and Poisson's ratio ν, show that our compounds have brittle aspects.

To estimate the elastic nature of the cubic $XGeO_3$ (X=Sr, Ca) perovskite oxides, the elastic anisotropy factor (A) has been studied as it gives the elasticity of the material in different directions. According to this, a material is isotropic, if the anisotropy factor (A) is equal to unity, and the deviation from unity indicates directly an anisotropic material aspect. Thus, the computed values of A are equal to 0.75 and 0.72 for $SrGeO_3$ and $CaGeO_3$, respectively. This result reveals the anisotropic nature of the studied materials [64].

3.3. Electronic properties

It is well known that the nature of materials can typically be determined based on their electronic band gap. In addition, the desirable applications of these materials in technology are induced by their experimentally or theoretically measured characteristic energy gap values. Therefore, we have analyzed the electronic properties of the $XGeO_3$ (X= Sr, Ca)

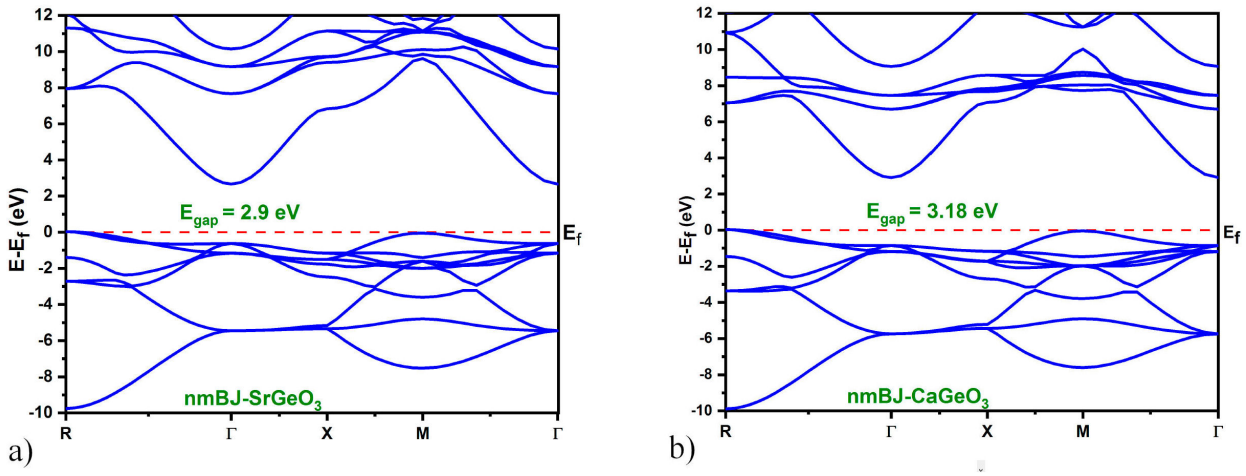

FIGURE 3. The Band structure of cubic perovskite oxides $XGeO_3$ (X= Sr, Ca).

TABLE III. Calculated values of bulk modulus B, shear modulus G, Pugh's ratio B/G, Young's modulus Y, Cauchy pressure C'', Poisson's ratio ν and elastic anisotropic factor A of the cubic $XGeO_3$ (X=Sr, Ca) perovskite oxides, comparing with other theoretical works.

Parameters	$SrGeO_3$	$CaGeO_3$	[49]	[51]
B(GPa)	190.21	173.54	178	156.32
G(GPa)	132.69	110.34	123.07	98.67
B/G	1.43	1.57	1.448	1.58
Y(GPa)	322.98	273.13	112.54	244.56
C''(GPa)	-35	-13.4	-31	-17.34
ν	0.22	0.24	0.219	0.239
A	0.75	0.72	1.531	0.967

materials based on band structure, the total density of state (TDOS), and partial density of state (PDOS) using nmBJ approximation.

According to Fig. 2, which illustrates the band structure of $XGeO_3$ (X= Sr, Ca) perovskite oxides, it is obvious that the highest point of the valence band (VB) is placed at the M symmetric point, while the lower point of the conduction band (CB) is on Γ symmetric point for both materials. As a consequence, this result indicates that our compounds have a semiconductor nature with indirect band gap $(\Gamma - M)$. For the first material $SrGeO_3$, the band gap value is equal to 2.9 eV, while $CaGeO_3$ element has a band gap value equal to 3.18 eV, according to other theoretical works [4, 51, 65].

To comprehend and clarify the obtained results about the band structure of our materials $XGeO_3$ (X= Sr, Ca), we have studied and determined their total density of state (TDOS) and their partial density of state (PDOS), as presented in Fig. 3. From this figure, we remark that the s and p orbitals of Germanium are dominant for the energies below -4 eV in the valence band (VB) for the two materials. For the $SrGeO_3$ material, we observe various states with small factors coming from $(p,\ d)$ states of Strontium and $d - states$ of Germanium. For the $CaGeO_3$ material, we have also a small contribution coming from the d state of Calcium and Germanium in the region -4 eV to the Fermi level. However, the p orbitals of oxygen show a strong effect in this region as compared to the other states for both materials. In the conduction band (CB), it is clear that the orbital responsible for the band gap energy in the two materials is the s orbital corresponding to the Germanium atom. This result confirms the semiconductor nature of our compounds $XGeO_3$ (X= Sr, Ca).

3.4. Spontaneous polarization properties

In this part, we investigated the ferroelectric properties of the studied materials. The spontaneous polarization (P_s) is regarded as a fundamental characteristic of ferroelectric materials, defined as the change in polarization that occurs when the crystal undergoes a phase transition from a centrosymmetric structure to a structure without inversion symmetry. For a given state, the polarization of materials consists of two components, the first depends on the spatial distribution of the electron density, and the second part is ionic, based on the displacement of ion or atom immigrations.

Based on Berry phase BI approach introduced in the Wien2k code, we computed the spontaneous polarization of both cubic perovskite oxides $XGeO_3$ (X=Sr, Ca). Our study of the P_s involves two distinct calculations: one for the centro symmetric structure (unperturbed) and the other for

TABLE IV. Calculated values of the spontaneous polarization P_s in various strains for the cubic $XGeO_3$ (X=Sr, Ca) perovskites oxides, comparing with other works.

Compounds	c/a	P_s(C/m^2)
$SrGeO_3$	1	$6.707453\ 10^{-15}$
	1.006	$2.469515\ 10^{-1}$
	1.013	$2.479767\ 10^{-1}$
	1.020	$2.493217\ 10^{-1}$
$CaGeO_3$	1	$7.331402\ 10^{-15}$
	1.013	$2.463986\ 10^{-1}$
	1.026	$2.486206\ 10^{-1}$
	1.039	$2.507034\ 10^{-1}$
$BaTiO_3$	1.011	0.320
$PbTiO_3$	1.0635	0.8844
$BaHfO_3$	-	0.40

the non-centrocymmetric structure (perturbed). For the perturbed structure, we introduced various displacements in the c-parameter of our study materials to investigate their effect on the spontaneous polarization. Table IV displays the spontaneous polarization of $XGeO_3$ (X=Sr, Ca) materials for three different displacements on the c-parameter. For both materials, we observe that the (P_s) is nearly zero in the unperturbed structure. However, the displacement in the c-parameter changes the cell volume of cubic $XGeO_3$ (X=Sr, Ca) perovskites. Consequently, the charge density increases, indicating the emergence of spontaneous polarization, as shown in Table IV. According to this table, the (P_s) increases by increasing the external effect. We notice that, the obtained value for P_s is in good agreement compared to other perovskite oxides family, such as $BaTiO_3$, $PbTiO_3$ and $BaHfO_3$ [66–68].

Finally, our proposed perovskite materials present important values of spontaneous polarization, indicating their excellent ferroelectric behavior. This characteristic makes these materials strong and good candidates for the development of ferroelectric devices.

3.5. Thermodynamic properties

In this part, we have investigated the thermodynamic properties of the cubic $SrGeO_3$ and $CaGeO_3$ compounds using the Gibbs2 program within the quasi-harmonic approximation. As it is well-known, the Gibbs function, in the Debye approach, is expressed as follows [69, 70]:

$$G(V,P,T) = E(V) + PV + F_v(\theta_D,T), \qquad (13)$$

where $E(V)$ is the energy per unit cell, and $F_v(\theta_D,T)$ is the vibration function which is given by:

$$F_v(\theta_D,T) = NK_BT\left(\frac{9\theta_D}{8T} + 3\ln\left[1-e^{(-\theta_D/T)}\right] - D\left[\frac{\theta_D}{T}\right]\right). \qquad (14)$$

For a solid material, θ_D is the Debye temperature, and it is expressed as follows:

$$\theta_D = \frac{h}{K_B}(6\pi^2V^{1/2}N)^{1/3}f(\nu)\sqrt{\frac{B}{M}}, \qquad (15)$$

where M is the atoms mass, and B is the bulk modulus per unit cell such that:

$$B = V\left(\frac{d^2E(V)}{dV^2}\right). \qquad (16)$$

In addition, there are also other interesting thermodynamic quantities such as heat capacities (C_V and C_P), expansion coefficient α, Grüneisen parameter γ, and entropy S. Mathematically, these quantities are successively expressed by the following equations:

$$C_V = 3NK_B\left(4D\left[\frac{\theta_D}{T}\right] - \frac{3\frac{\theta_D}{T}}{\exp\frac{\theta_D}{T}-1}\right), \qquad (17)$$

$$C_P = C_V(1+\gamma\alpha T), \qquad (18)$$

$$\alpha = \frac{\gamma C_V}{BV}, \qquad (19)$$

$$\gamma = -\frac{d\ln(\theta_D(V))}{\ln(V)}, \qquad (20)$$

$$S = NK_B\left(4D\left[\frac{\theta_D}{T}\right] - 3\ln\left[1-\exp\frac{-\theta_D}{T}\right]\right), \qquad (21)$$

where $D(\theta_D/T)$ is the Debye integral.

Here, we report the thermodynamic properties of the $SrGeO_3$ and $CaGeO_3$ compounds. These properties are evaluated for temperatures ranging from 0 K to 1000 K and for pressures between 0 GPa and 20 GPa. The choice of both ranges of temperature and pressure is based on the fact that the quasi-harmonic Debye approximation theory remains valid in these ranges. In addition, the lattice constant, bulk modulus, heat capacities, volume expansion coefficient, thermal expansion coefficient, Debye temperature, Gibbs free energy, enthalpy, and the Grüneisen parameter are investigated using the Gibbs2 program within the wien2k code. Figure 4 shows the direct dependence of unit cell volume of simple cubic perovskite oxides $SrGeO_3$ and $CaGeO_3$ on pressure and temperature. From this figure, we observe an increasing unit cell volume versus temperature at different pressures. This result is logical and generally common in solid materials, because when the temperature increases, the volume also increases immediately.

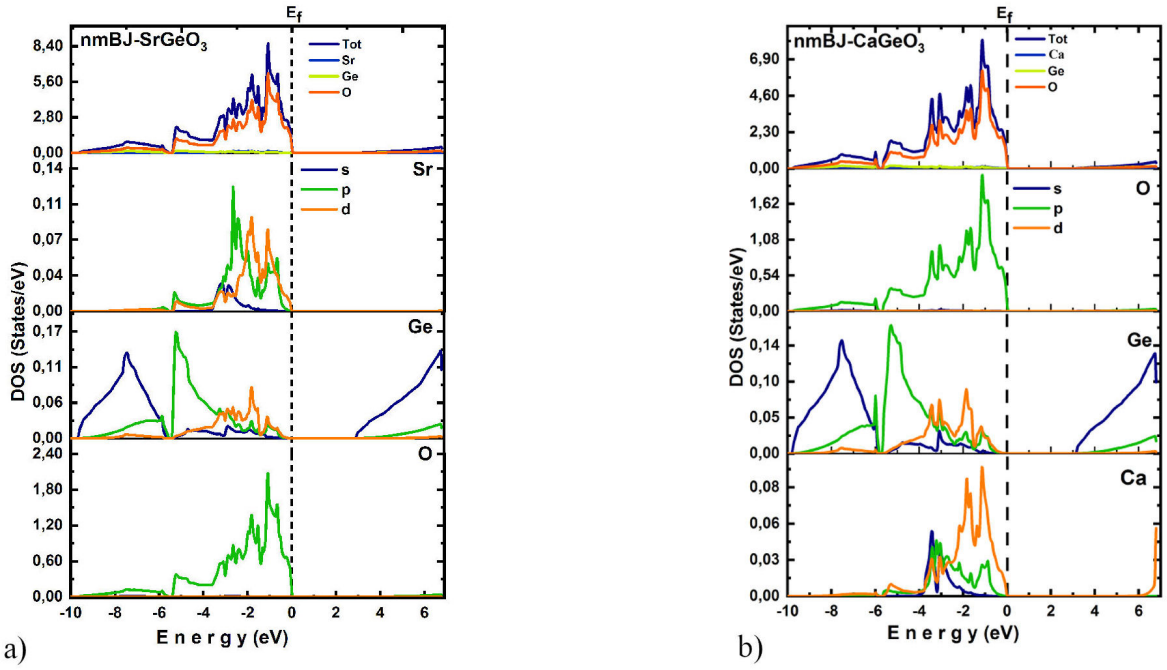

FIGURE 4. Total density of states (TDOS) and partial density of states (PDOS) of cubic $XGeO_3$ (X=Sr, Ca) perovskite oxides.

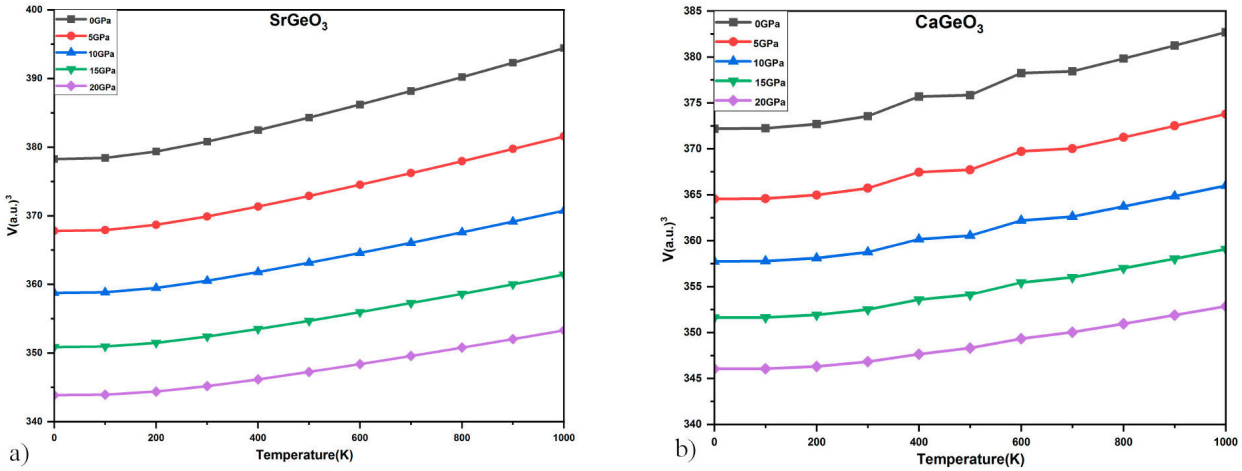

FIGURE 5. The dependence of unit cell volume of cubic perovskites oxides $SrGeO_3$ et $CaGeO_3$ on pressure and temperature.

The bulk modulus B is one of the critical properties that describes the deformation of a solid under pressure. The study of bulk modulus B of compression provides information about the dilatation of solid materials. It is also a measure of the capacity of a material to tolerate the changes in volume under compression. Figure 5 presents the dependence of bulk modulus B on pressure and temperature. From this figure, it is clear that bulk modulus B is changes due to the temperature and pressure effects. In addition, the bulk modulus is almost constant at low temperatures ($T < 120$ K), but when temperature increases ($T > 120$ K), the bulk modulus changes regardless of the considered pressure. Therefore, the bulk modulus B decreases with increasing temperature and decreasing pressure. Moreover, the inter-atomic distance in the crystal increases with increasing temperature, which leads to increasing crystal volume. Thereby, the bulk modulus B decreases with increasing volume. As a result, when the bulk modulus B increases, the compressibility of our materials decrease, which means that the resistance of both materials to deformation increase. From the analysis of the B parameter, it is clear that our compounds are hard and rigid under high pressure.

In general terms, both heat capacities at constant volume C_V and constant pressure C_P are significant features of a substance. They are interpreted as the amount of energy required to raise the temperature of a substance by one Kelvin (or degree Celsius). Figure 6 presents the dependence of heat capacitie (C_V) of both $SrGeO_3$ and $CaGeO_3$ compounds on

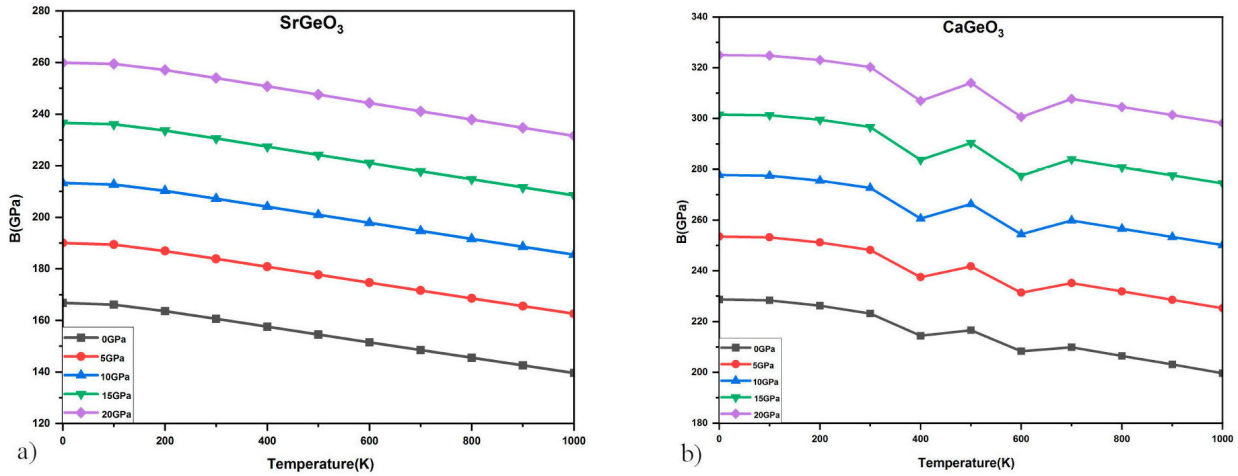

FIGURE 6. The dependence of the bulk modulus B of cubic perovskites oxides $SrGeO_3$ et $CaGeO_3$ compounds on pressure and temperature.

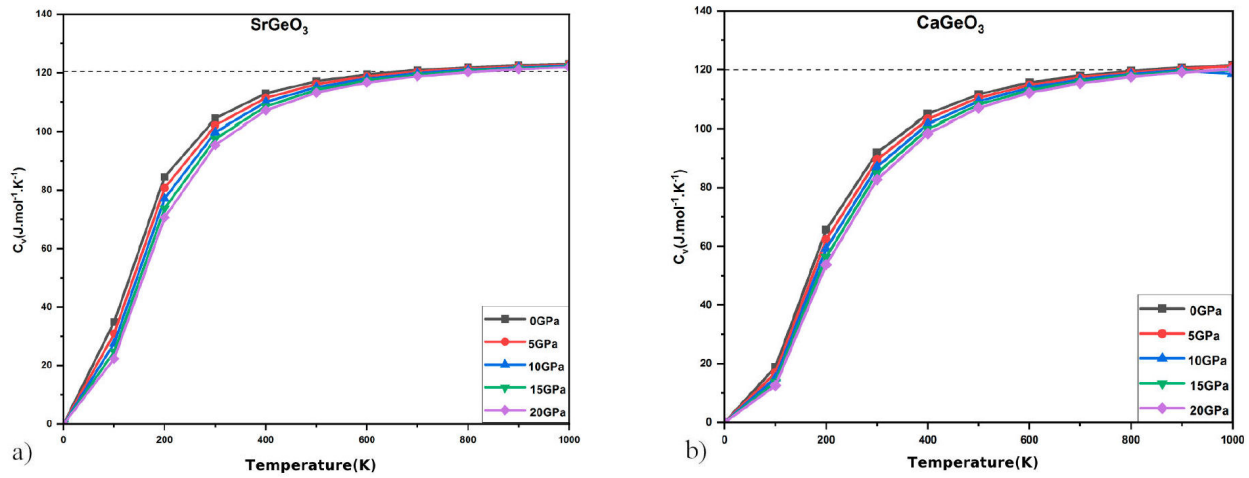

FIGURE 7. Variations of the heat capacitie C_V of cubic perovskites oxides $SrGeO_3$ and $CaGeO_3$ as a function of pressure and temperature.

temperature (form 0 K to 1000 K) and pressure (from 0 GPa to 20 GPa). At low temperatures below 300 K, both materials have an increasing C_V when the temperature increases, which means that the specific heat capacities present a robust dependence on temperature due to the Debye model. In addition, the temperature has a strong effect on the heat capacities as compared to that of the pressure. However, at high temperatures, the C_V curves approach the Dulong-Petit limit [71], and it is clear from the figure that all the curves of heat capacities become approximately aligned in this temperature region. Therefore, the effect of both pressure and temperature becomes negligible above the Dulong-Petit limit.

Figure 7 illustrates the variation of the thermal expansion coefficient (α) as a function of temperature at different pressures. It can be seen that the thermal expansion (α) increases exponentially with temperature less than 300 K. However, for temperatures higher than 300 K, we observe a slow and linear increase of the thermal expansion, corresponding to the quasi-harmonic approximation at high-temperature limit. At the same time, the thermal expansion coefficient values (α) of $SrGeO_3$ and $CaGeO_3$ at high pressures are smaller than those at low pressures. These results indicate the deficiency of the quasi-harmonic approximation at high temperatures and low pressures. Besides, the thermal expansion (α) is interpreted as the tendency of the matter phase to be modified under the variation of temperature and pressure, and it has also an effect on the melting point of solids. Therefore, high melting point materials are more likely to have a lower thermal expansion coefficient (α) [72]. Based on these results, our materials have small values of thermal expansion coefficient, which indicates that our materials have a high melting point, meaning a good hardness.

In solid state physics, the Debye temperature is a crucial quantity that describes the collective vibrational behaviour of atoms in a crystal lattice. It effectively describes the continuum of vibrational modes in a solid. A limited number of low-frequency vibrational modes are active at temperatures well below the Debye temperature. Increasing the Debye temperature leads to the excitation of additional vibrational modes. In addition, the Debye temperature (Θ_D) of materi-

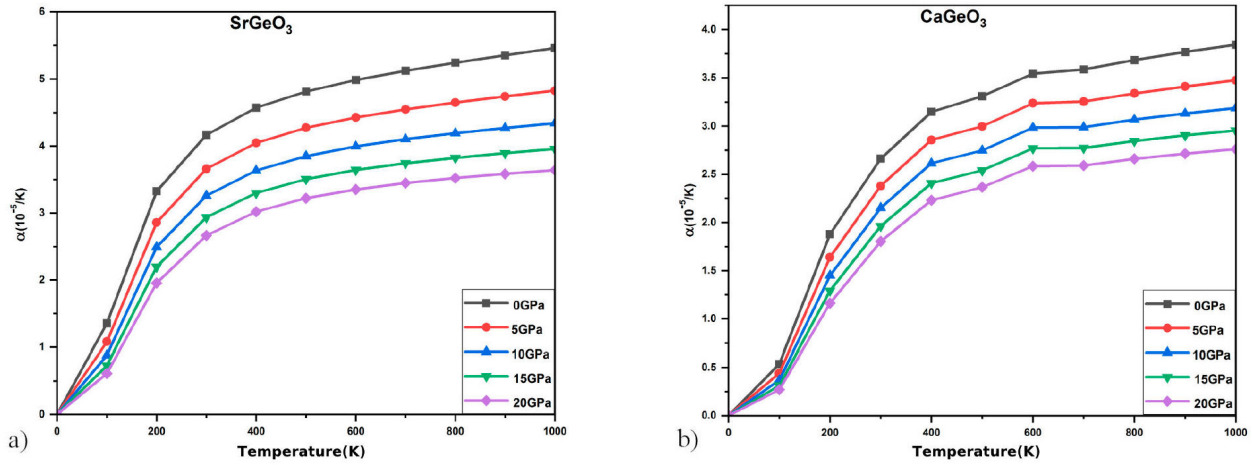

FIGURE 8. Thermal expansion coefficient (α) of cubic perovskites oxides $SrGeO_3$ and $CaGeO_3$ versus pressure and temperature.

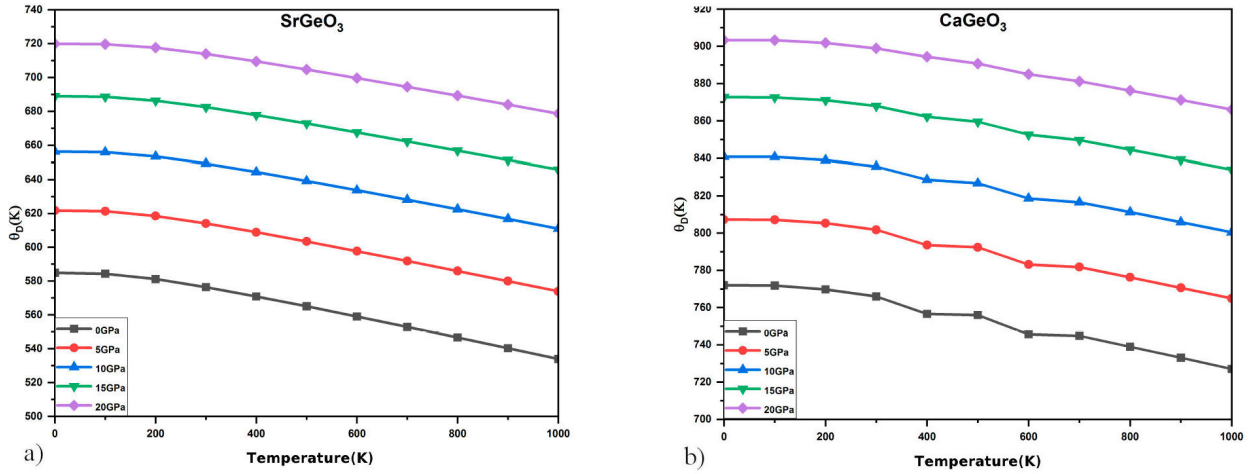

FIGURE 9. The dependence of the Debye temperature (Θ_D) of cubic perovskites oxides $SrGeO_3$ et $CaGeO_3$ on pressure and temperature.

als has played an important role in many physical properties of solids. The variation of the Debye temperature with respect to temperature and pressure is presented in Fig. 8. From this figure, it can be seen that the Debye temperature (Θ_D) decreases slowly with increasing temperature and increases strongly with pressure. Thus, the effect of pressure is greater than that of temperature. As a result, high values of the Debye temperature indicate a strong bond between atoms in the crystal, meaning our materials $SrGeO_3$ and $CaGeO_3$ have high melting temperature and hardness behavior. Whenever the pressure increases, the Θ_D of our compound increases, and this leads to a decrease in the inter-atomic distance [73]. In general, the Debye temperature is an essential quantity that helps us to understand the thermal and vibrational properties of crystalline materials.

The Grüneisen parameter is a key parameter in condensed matter physics that characterizes the thermal expansion and compressibility of a material. It is denoted by the symbol (γ) and is defined as the ratio of the relative change in volume of the relative change in temperature at each pressure. Physically, the Grüneisen parameter provides insights into how a material's lattice structure responds to changes in temperature, indicating whether it expands or contracts under heating. From Fig. 9, it is clear that when the temperature and pressure increase the Grüneisen parameter decreases, especially for the pressure above 5 GPa. However, it became approximately constant for 5 GPa, and it increases with temperature in 0 GPa. This result confirms the rigid nature and hardness behavior of our materials in a small pressure. In terms of vibrational modes, it is related to the anharmonicity of the crystal lattice. Generally, a positive Grüneisen parameter suggests that the material expands upon heating, while a negative value implies contraction. All this information is useful in understanding the thermodynamic properties of materials, especially in the context of phase transitions and thermal transport phenomena [74].

Entropy is one of the most important parameters in thermodynamics. It is used to describe the equilibrium state of thermodynamic systems (systems disorder). In Fig. 10, the entropy S of our compounds $SrGeO_3$ and $CaGeO_3$ is also

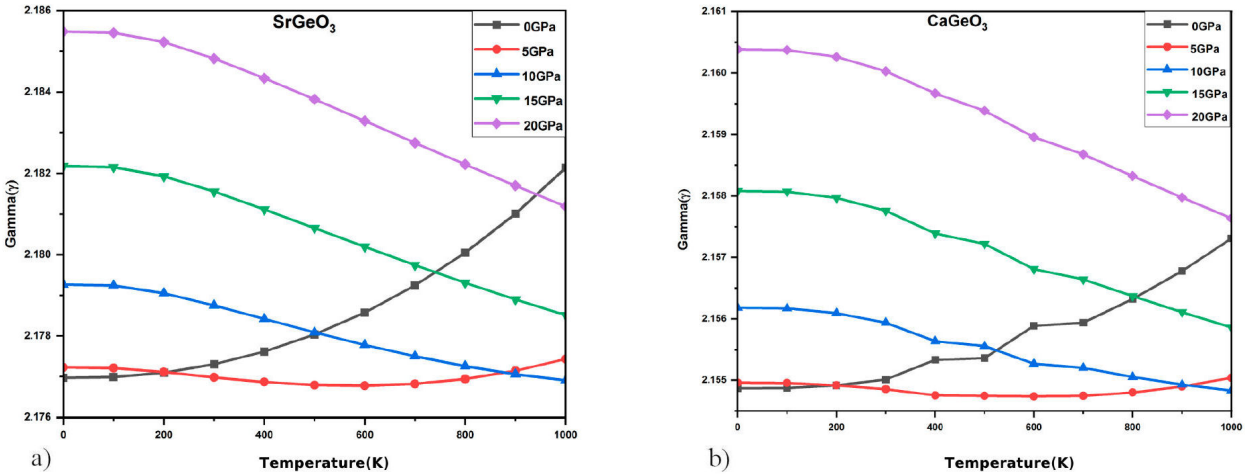

FIGURE 10. The dependence of the Grüneisen parameter (γ) of cubic perovskites oxides $XGeO_3$ (X= Sr, Ca) compound on pressure and temperature

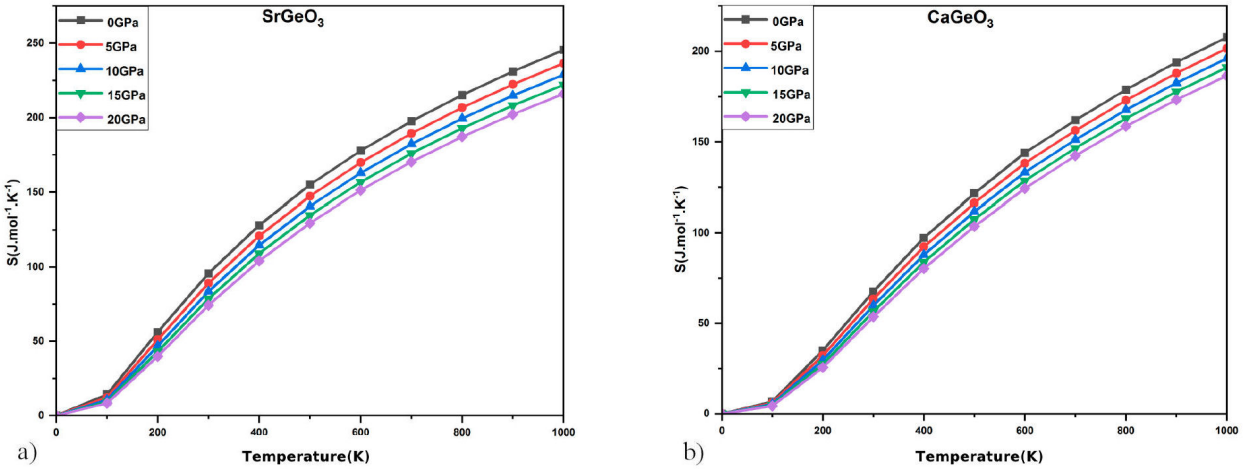

FIGURE 11. Variation of the entropy S of cubic perovskites oxides $XGeO_3$ (X= Sr, Ca) as a function of pressure and temperature.

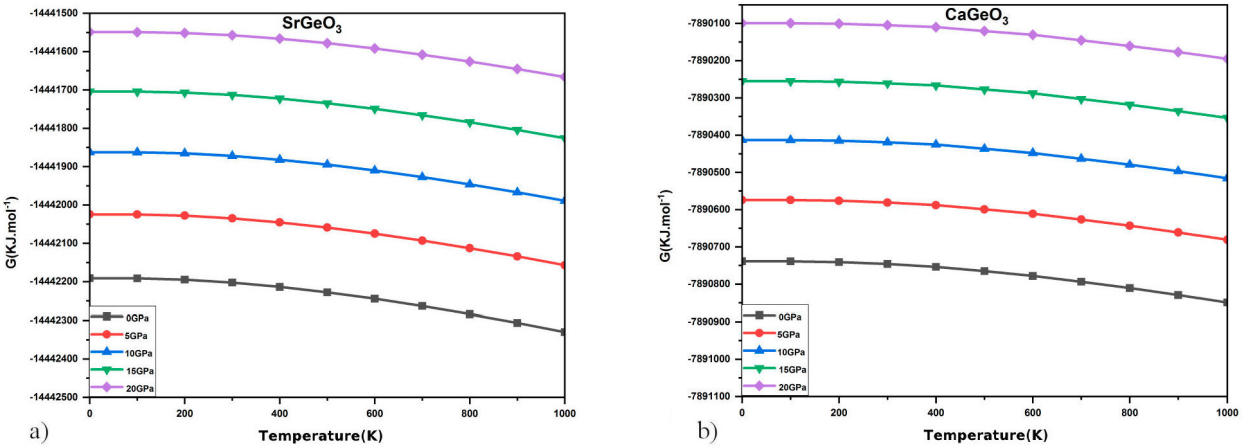

FIGURE 12. The dependence of the Gibbs free energy (G) of cubic perovskites oxides $SrGeO_3$ and $CaGeO_3$ compounds on pressure and temperature.

computed at different pressures from 0.0 to 20 GPa (with a step 5.0 GPa) and at different temperatures from 0 to 1000 K (with a step of 100 K). It is also interesting to note that the entropy S increases with increasing temperature and slowly decreases with pressure. These can be explained qualitatively by considering the fact that at high temperatures, the entropy increases at any given pressure. Which means, the number of phonon modes is increased and the vibrational contribution to the entropy increases when the temperature increases. As a result, the pressure causes that our materials $SrGeO_3$ and $CaGeO_3$ become more ordered, while the temperature makes them disordered [54].

In thermodynamics, Gibbs free energy which is known as a free enthalpy is utilized to compute the maximum quantity of work done in a thermodynamic system when the temperature and pressure are constant. It can be explained also as the quantity of useful energy present in a thermodynamic system. In Fig. 11, we have treated the dependence of the Gibbs free energy for the simples cubic perovskite oxides $SrGeO_3$ and $CaGeO_3$ on the temperature and pressure. One can see that the Gibbs free energy is approximately constant for temperatures below 400 K. However, when the temperature increases above 400 K, the Gibbs energy begins to decrease for different pressures. Moreover, the Gibbs free energy of our materials increases significantly whenever the pressure increases. Therefore, the Gibbs free energy of these compounds results more strongly affected by pressure than temperature.

4. Conclusion

Structural, dynamic, mechanical, electronic, spontaneous poarization, and thermodynamic properties of $XGeO_3$ (X = Sr, Ca) perovskites have been calculated with density functional theory as incorporated in WIEN2K. The tolerance factor is equal to 0.945 and 0.911 for $SrGeO_3$ and $CaGeO_3$, respectively, indicating that both materials have a stable cubic structure. In addition, the no imaginary frequencies in the phonon disperation curve show the dynamical stability of the compounds in a cubic phase. Moreover, the calculated elastic constants show the mechanical stability of the studied perovskites which respect to Born criteria. A britle and anisotropic aspects have been proved through the obtained mechanical parameters. Furthermore, the computed electronic properties prove that the $SrGeO_3$ and $CaGeO_3$ materials display a p-type semiconductor nature with an indirect band gap value equal to 2.9 eV and 3.18 eV , respectively. Additionally, the high values 0.249 and 0.251 C/m^2 of the spontaneous polarization show a ferroelctric behavior, respectively, for $SrGeO_3$ and $CaGeO_3$. Finally, the applied temperature (0 to 1000 K) and pressure (0 to 20 GPa) have been found to make great changes in the thermodynamic parameters such as volume cell, bulk modulus, thermal expansion coefficient, Debye temperature, Gibbs free energy, enthalpy, heat capacities, and Grüneisen parameter. All treated properties of $XGeO_3$ (X = Sr, Ca) highlighted that these studied materials have a wide range of application in ferroelectruic devices, such as sensors, radio frequency filters, and non-volatile memories.

1. A.E. Katz, Perovskite: Name Puzzle and German-Russian Odyssey of Discovery, *Helvetica Chimica Acta* **103** (2020) e2000061, https://doi.org/10.1002/hlca.202000061.
2. A. Abbassi *et al*., Magneto-Thermal, Mechanical, and Optoelectronic Properties of Sr_2MWO_6 (M = V , Rh, Ru): Ab Initio Study, *J. Supercond. Nov. Magn*. **36** (2023) 995-1001, https://doi.org/10.1007/s10948-023-06537-0.
3. M. Agouri *et al*., Insight into the effect of rare earth RE = Ce, Nd, Gd elements on the physical properties of Pb-Based Perovskite Oxides ($PbREO_3$), *Mater. Sci. Eng. B*. **294** (2023) 116550, https://doi.org/10.1016/j.mseb.2023.116550.
4. A. Waqdim *et al*., Theoretical investigation of the physical properties of cubic perovskite oxides $SrXO_3$ (X = Sc, Ge, Si), *Mater. Sci. Semicond*. **158** (2023) 107340, https://doi.org/10.1016/j.mssp.2023.107340.
5. A. Zaghrane *et al*., First-principles investigation of structural, electronic, optical, and magnetic properties of a scintillating double perovskite halides (Cs_2LiCeX_6) with (X = F, Br, and I), *Chin. J. Phys*. (2023). https://doi.org/10.1016/j.cjph.2023.08.001.
6. R. E. Cohen, Origin of ferroelectricity in perovskite oxides, *Nature*. **358** (1992) 136, https://doi.org/10.1038/358136a0.
7. P. G. Silvestrov, *et al.*, Polarized electric current in semiclassical transport with spin-orbit interaction, *Phys. Rev. B.* **74** (2006) 165301, https://doi.org/10.1103/PhysRevB.74.165301.
8. R. Sharif *et al*., A comprehensive review of the current progresses and material advances in perovskite solar cells, *Nanoscale Adv*. **5** (2023) 3803, https://doi.org/10.1039/D3NA00319A.
9. C. S. Hwang *et al*., Advances in Non-Volatile Memory and Storage Technology, (Woodhead Publishing Series in Electronic and Optical Materials, 2019), p.p. 393-441, https://doi.org/10.1016B978-0-08-102584-0.00012-7.
10. I. Grinberg, *et al.*, Perovskite oxides for visible-light-absorbing ferroelectric and photovoltaic materials, *Nature* **503** (2013) 509-512, https://doi.org/10.1038/nature12622.

11. X. Luo *et al*., Electron transport enhancement of perovskite solar cell due to spontaneous polarization of Li^+ -doped $BaTiO_3$, *Solid State Sci*. **108** (2020) 106387, https://doi.org/10.1016/j.solidstatesciences.2020.106387.

12. H.S. Bhatti, *et al.*, Synthesis and induced multiferroicity of perovskite $PbTiO_3$; a review, *Appl. Surf. Sci*. **367** (2016) 291, https://doi.org/10.1016/j.apsusc.2016.01.164.

13. Z. Pan, *et al.*, Large spontaneous polarization in polar perovskites of $PbTiO_3$-$Bi(Zn_{1/2}Ti_{1/2})O_3$, *Inorg. Chem. Front*. **5** (2018) 1277, https://doi.org/10.1039/C8QI00184G.

14. C. He, *et al*., Inorganic photovoltaic cells based on $BiFeO_3$: spontaneous polarization, lattice matching, light polarization and their relationship with photovoltaic performance, *Phys. Chem. Chem. Phys*. **22** (2020) 8658, https://doi.org/10.1039/D0CP01176B.

15. X.K. Wei, *et al*., Polarity of translation boundaries in antiferroelectric $PbZrO_3$, *Mater. Res. Bull*. **62** (2015) 101-105, https://doi.org/10.1016/j.materresbull.2014.11.024.

16. A. Savage, Pyroelectricity and Spontaneous Polarization in $LiNbO_3$, *J. Appl. Phys*. **37**, (1966) 3071-3072, https://doi.org/10.1063/1.1703164.

17. Y. Zhang *et al.*, Strain tunable ferroelectric and dielectric properties of $BaZrO_3$, *J. Appl. Phys*. **115** (2014) 224107, https://doi.org/10.1063/1.4883298.

18. L. G. Ferreira *et al*., Ferrielectric Twin Walls in $CaTiO_3$, *PRL* **101** (2008) 097602, https://doi.org/10.1103/PhysRevLett.101.097602.

19. A. Abbassi *et al.*, Spontaneous Polarization and Magnetic Investigation Of $BiXO_3$ (X=Co, Mn, Fe, V, Zn): First-Principle Study, *J. Supercond. Nov. Magn*. **29** (2015) 487, https://doi.org/10.1007/s10948-015-3315-z.

20. C. Azahaf *et al.*, Theoretical investigation of spontaneous polarization, electronic and optical properties of cubic perovskite $BaHfO_3$, *Opt Quant Electron.* **47** (2015) 2889, https://doi.org/10.1007/s11082-015-0178-2.

21. R. Chiara *et al*, Germanium-Based Halide Perovskites: Materials, Properties, and Applications, *ChemPlusChem*. **86** (2021) 879, https://doi.org/10.1002/cplu.202100191.

22. K. Ding, *et al.*, Superior ferroelectricity and nonlinear optical response in a hybrid germanium iodide hexagonal perovskite, *Nat. Commun*. **14**, (2023) 2863, https://doi.org/10.1038/s41467-023-38590-7.

23. S. Bouhmaid *et al.*, A DFT study of electronic, optical and thermoelectric properties of Ge-halide perovskites $CsGeX_3$ (X=F, Cl and Br), *Comput. Condens. Matter.* **31** (2022) e00663 https://doi.org/10.1016/j.cocom.2022.e00663.

24. A. Dey *et al.*, Cubic PbGeO3 perovskite oxide: A compound with striking electronic, thermoelectric and optical properties, explored using DFT studies, *Comput. Condens. Matter*. **26** (2021) e00532, https://doi.org/10.1016/j.cocom.2020.e00532.

25. W. Xiao *et al.*, A new cubic perovskite in PbGeO3 at high pressures, *Am. Min.* **97** (2012) 1193, https://doi.org/10.2138/am.2012.4021.

26. N. A. Noor *et al.*, Physical properties of cubic $BaGeO_3$ perovskite at various pressure using first-principle calculations for energy renewable devices, *J. Mol. Graph. Model*. **84** (2018) 152, https://doi.org/10.1016/j.jmgm.2018.06.020.

27. A. Nakatsuka *et al*., Crystal structure of $SrGeO_3$ in the high-pressure perovskite-type phase, *Acta Cryst*. **71** (2015) 502, https://doi.org/10.1107/S2056989015007264.

28. J. Cheng *et al*., Design of two-dimensional electron gas systems via polarization discontinuity from large-scale first-principles calculations, *J. Mater. Chem. C* **6** (2018) 6680-6690, https://doi.org/10.1039/C8TC01893F.

29. Y. Wang *et al*., High-mobility two-dimensional electron gas in $SrGeO_3$- and $BaSnO_3$-based perovskite oxide heterostructures: an ab initio study, *Chem. Chem. Phys.* **18** (2016) 31924-31929, https://doi.org/10.1039/C6CP05572A.

30. Q. Q. Ye *et al*., A $SrGeO_3$ inorganic electron-transporting layer for highperformance perovskite solar cells, *Mater. Chem. A* **7** (2019) 14559, https://doi.org/10.1039/C9TA03176F.

31. A. Nakatsuka *et al*., A $SrGeO_3$ inorganic electron-transporting layer for high-performance perovskite solar cell, *Journal of mineralogical and petrological sciences* **113**, (2018) 280-285, https://doi.org/10.2465/jmps.180605.

32. R. B. Behram *et al*., Ab-initio investigation of $AGeO_3$ (A = Ca, Sr) compounds via Tran-Blaha-modified Becke-Johnson exchange potential *Chin. Phys. B* **26** (2017) 116103, https://doi.org/10.1088/1674-1056/26/11/116103.

33. R. M. Dreizler and E. K. U. Gross, Density Functional Theory (Springer, 1990), https://doi.org/10.1007/978-3-642-86105-5.

34. R. G. Parr and Y. Weitao, Density-Functional Theory of Atoms and Molecules, (Oxford University Press, 1994). https://doi.org/10.1007/978-3-319-14045-2_37

35. P. Blaha *et al*., Full-potential, linearized augmented plane wave programs for crystalline systems, *Comput. Phys. Commun*. **59** (1990) 399, https://doi.org/10.1016/0010-4655(90)90187-6

36. J. P. Perdew, *et al*., Restoring the Density-Gradient Expansion for Exchange in Solids and Surfaces, *Phys. Rev. Lett*. **102**, (2009) 039902, https://doi.org/10.1103/PhysRevLett.100.136406.

37. F. Tran, *et al*., Accurate Band Gaps of Semiconductors and Insulators with a Semilocal Exchange-Correlation Potential, Phys. Rev. Lett. **102**, (2009) 226401, https://doi.org/10.1103/PhysRevLett.102.226401

38. D. Koller, *et al*., Improving the modified Becke-Johnson exchange potential, *Phys. Rev.B.* **85**, (2012) 155109, https://doi.org/10.1103/PhysRevB.85.155109.

39. H. J. Monkhorst and J. D. Pack, Special points for Brillouin-zone integrations, *Phys. Rev. B.* **13** (1976) 5188, https://doi.org/10.1103/PhysRevB.13.5188

40. F. Birch, The Effect of Pressure Upon the Elastic Parameters of Isotropic Solids, According to Murnaghan's Theory of Finite Strain, *J. Appl. Phys.* **9** (1938) 279, https://doi.org/10.1063/1.1710417

41. A. Togo and I. Tanaka, First principles phonon calculations in materials science, *Scr. Mater.* **108** (2015) 1-5, https://dx.doi.org/10.1016/j.scriptamat.2015.07.021.

42. R. Golesorkhtabar *et al.*, ElaStic: A tool for calculating second-order elastic constants from first principles, *Computer Physics Communications.* **184** (2013) 1861, https://doi.org/10.1016/j.cpc.2013.03.010.

43. S. J. Ahmed *et al*., BerryPI: A software for studying polarization of crystalline solids with WIEN2k density functional all-electron package, *Computer Physics Communications.* **184** (2013) 647-651, https://doi.org/10.1016/j.cpc.2012.10.028.

44. S. A. Dar, V. Srivastava, U. K. Sakalle, Ab Initio High Pressure and Temperature Investigation on Cubic $PbMoO_3$ Perovskite, *J. Electron. Mater*. **46** (2017) 6870, https://doi.org/10.1007/s11664-017-5731-2.

45. M. A. Blanco *et al., J. Mol. Struct. Theochem.* **268** (1996), https://doi.org/10.1016/j.mseb.2018.12.007.

46. M. A. Blanco *et al*., E. Francisco and V. Luaña, GIBBS: isothermal-isobaric thermodynamics of solids from energy curves using a quasi-harmonic Debye model, *Phys. Commun.* **57** (2004) 158, https://doi.org/10.1016/j.comphy.2003.12.001.

47. K. Momma and F. Izumi, VESTA3 for three-dimensional visualization of crystal, volumetric and morphology data, *J. Appl. Cryst*. **44** (2011) 1272, https://doi.org/10.1107/S0021889811038970.

48. F. D. Murnaghan, The Compressibility of Media under Extreme Pressures, *PNAS* **30** (1994) 244, https://doi.org/10.1073/pnas.30.9.244.

49. C. A. Niedermeier *et al.*, covering condensed matter and materials physics Phonon scattering limited mobility in the representative cubic perovskite semiconductors $SrGeO_3$, $BaSnO_3$, and $SrTiO_3$, *Phy. Rev. B.* **101** (2020) 125206, https://doi.org/10.1103/PhysRevB.101.125206.

50. C. H. Kronbo *et al*., High pressure structure studies of three $SrGeO_3$ polymorphs - Amorphization under pressure, *Journal of alloys and compounds* **885** (2021) 157419, https://doi.org/10.1016/j.jallcom.2020.157419.

51. R. B. Behram *et al*., *Chin. Phys. B* **26** (2017) 116103, https://doi.org/10.1088/1674-1056/26/11/116103.

52. V. M. Goldschmidt, Die Gesetze der Krystallochemie, *Naturwissenschaften* **14** (1926) 477, https://doi.org/10.1007/BF01507527.

53. Z. Li *et al*, Stabilizing Perovskite Structures by Tuning Tolerance Factor: Formation of Formamidinium and Cesium Lead Iodide Solid-State Alloys, *Chem. Mater.* **28** (2016) 284-292, https://doi.org/10.1021/acs.chemmater.5b04107.

54. P. Kumari *et al*., DFT calculations of opto-electronic, mechanical, thermodynamic, and transport properties of XCeO3 (X = Mg, Ca, and Ba) perovskite, *J. Chem. Thermodynamics* **18** (2023) 107071, https://doi.org/10.1016/j.jct.2023.107071.

55. P. Kumari *et al* Exploration of optoelectronic, thermodynamic, and thermoelectric properties of $RFeO_3$ (R = Pr, Nd) perovskites, *Materials Science and Engineering B.* **299** (2024) 117044, https://doi.org/10.1016/j.mseb.2023.117044.

56. A. Nakatsuka, *et al*., Temperature dependence of crystal structure of CaGeO3 high-pressure perovskite phase and experimental determination of its Debye temperatures studied by low- and hightemperature single-crystal X-ray diffraction, *American Mineralogist* **100** (2015) 1190-1202, https://doi.org/10.2138/am-2015-4945.

57. M. Born, On the stability of crystal lattices, *I. Mathematical Proceedings of the Cambridge Philosophical Society,* **36** (1940) 160, https://doi.org/10.1017/S0305004100017138.

58. F. Mouhat and F.X. Coudert, Necessary and sufficient elastic stability conditions in various crystal systems, *Phys. Rev. B* **90** (2014) 224104, https://doi.org/10.1103/PhysRevB.90.224104.

59. A. Reuss, Berechnung der Fließgrenze von Mischkristallen auf Grund der Plastizitätsbedingung für Einkristalle, *Journal of Applied Mathematics and Mechanics* (1929), https://doi.org/10.1002/zamm.19290090104.

60. R. Hill, The Elastic Behaviour of a Crystalline Aggregate, *Proc. Phys. Soc. A* **65**, (1952) 349, https://doi.org/10.1088/0370-1298/65/5/307.

61. W. Voigt, Lehrbuch der Kristallphysik, (Taubner, Leipzig, 1928), https://doi.org/10.1007/978-3-663-15884-4.

62. S. F. Pugh, XCII. Relations between the elastic moduli and the plastic properties of polycrystalline pure metals. *The London, Edinburgh, and Dublin Philosophical Magazine and Journal of Science* **45** (1954) 823, https://doi.org/10.1080/14786440808520496.

63. I. N. Frantsevich, F. F. Voronov, and S. A. Bokuta, Elastic constants and elastic moduli of metals and insulators, (Kiev, Naukova dumka, 1982).

64. C. M. Kube, Elastic anisotropy of crystals, *AIP Advances*. **6** (2016) 095209, https://doi.org/10.1063/1.4962996.

65. J. M. Henriques *et al*., Ab initio structural, electronic and optical properties of orthorhombic $CaGeO_3$, *Journal of Solid State Chemistry* **180** (2007) 974, https://doi.org/10.1016/j.jssc.2006.12.029

66. Said Amounas *et al.*, Dependence of tetragonal barium titanate spontaneous polarization and refractive indices on DFT exchange-correlation functionals, *Physica B: Condensed Matter.* **674** (2024) 415536, https://doi.org/10.1016/j.physb.2023.415536.

67. C. Azahaf *et al*. Theoretical investigation of spontaneous polarization, electronic and optical properties of cubic perovskite $BaHfO_3$, *Opt Quant Electron.* **47** (2015) 2889, https://doi.org/10.1007/s11082-015-0178-2.

68. S. Amounas *et al.*, DFT investigation of lattice parameters, spontaneous polarization, and refractive indices of tetragonal $BaTiO_3$ and $PbTiO_3$, *Physica B: Condensed Matter.* **663** (2023) 415002, https://doi.org/10.1016/j.physb.2023.415002.

69. O. Sahnoun *et al*., Ab initio study of structural, electronic and thermodynamic properties of tungstate double perovskites Ba_2MWO_6 (M = Mg, Ni, Zn), *Comput. Mater. Sci.* **77** (2013) 316, https://doi.org/10.1016/j.commatsci.2013.04.053.

70. S. A. DAR *et al*., Ferromagnetic Phase Stability, Magnetic, Electronic, Elasto-Mechanical and Thermodynamic Properties of BaCmO3 Perovskite Oxide, *J. Electron. Mater.* **47** (2018) 3809, https://doi.org/10.1007/s11664-018-6251-4.

71. A. T. Petit and P. L. Dulong, Recherches sur Quelques Points Importants de la ThÃ©orie de la Chaleur, *Annales de Chimie et de Physique.* **10** (1819) 395,

72. J. Garai, Correlation between thermal expansion and heat capacity, *Calphad* **30** (2006) 354-356, https://doi.org/10.1016/j.calphad.2005.12.003.

73. Z. Guo *et al*., Effects of pressure and temperature on thermodynamic properties of WB3 by first-principles predictions, *Mat. Res. Express* **6** (2019) 115034, https://doi.org/10.1088/2053-1591/ab45b1.

74. L. Burakovsky and D. L. Preston, Analytic model of the Grüneisen parameter all densities, *J. Phys. Chem. Solids* **65** (2004) 1581-1587, https://doi.org/10.1016/j.jpcs.2003.10.076.